Botti et al., https://doi.org/10.1083/jcb.201610051

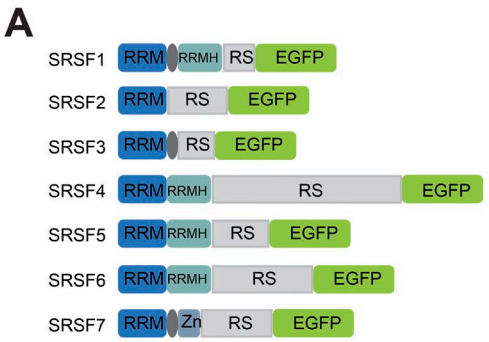

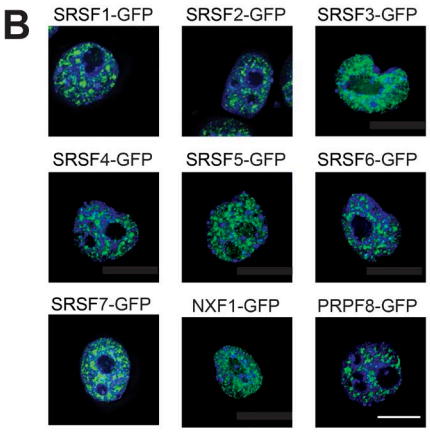

E

Protein	Shuttling capacity CHX(%)	Puro (%)
PRPF8	2.5	7.4
SRSF4	16.0	12.8
SRSF6	22.0	
SRSF2	29.9	26.0
SRSF5	31.0	
SRSF7	39.0	
SRSF1	39.5	36.7
SRSF3	40.0	44.8
NXF1	55.2	59.8

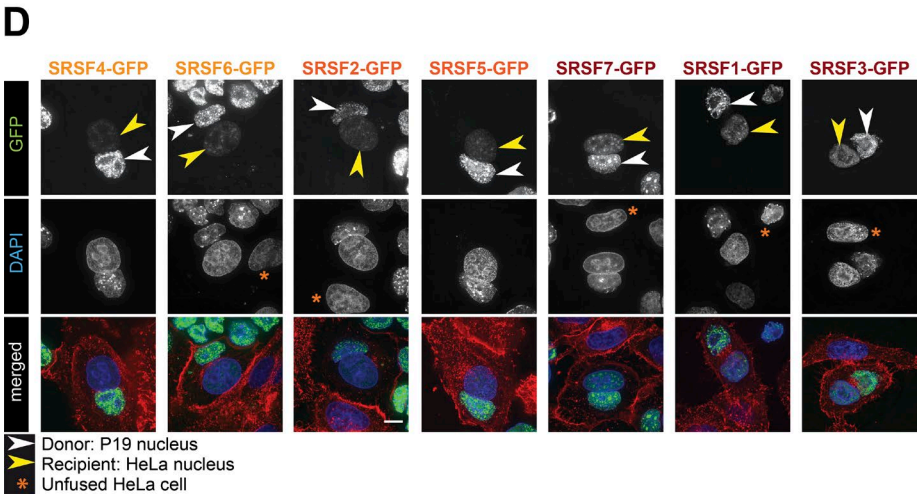

Figure S1. **Development of quantitative shuttling assays for SR proteins in pluripotent P19 cells (related to Fig. 1).** (A) Schema illustrating the domain structure of the seven GFP-tagged SR proteins used in this study. RRMH, RRM-homologous domain; RS, domain rich in arginine and serine residues; Zn, zinc knuckle. The gray oval indicates an NXF1-interacting domain (Hargous et al., 2006; Tintaru et al., 2007). (B) Merged fluorescence microscopy images confirming the predominantly nuclear localization of GFP-tagged SR proteins and the control proteins NXF1-GFP and PRPF8-GFP. Nuclei were stained with Hoechst. (C) GFP-tagged SR proteins are phosphorylated in vivo. Western blots show a decrease in the molecular weight of all GFP-tagged SR proteins after treatment with shrimp alkaline phosphatase (SAP). GFP-NLS was used as negative control. (D) Additional examples of heterokaryons used for quantification. Bars, 10 µm. (E) Shuttling assays performed in the presence of CHX or puromycin (Puro) to inhibit translation resulted in similar median shuttling capacities.

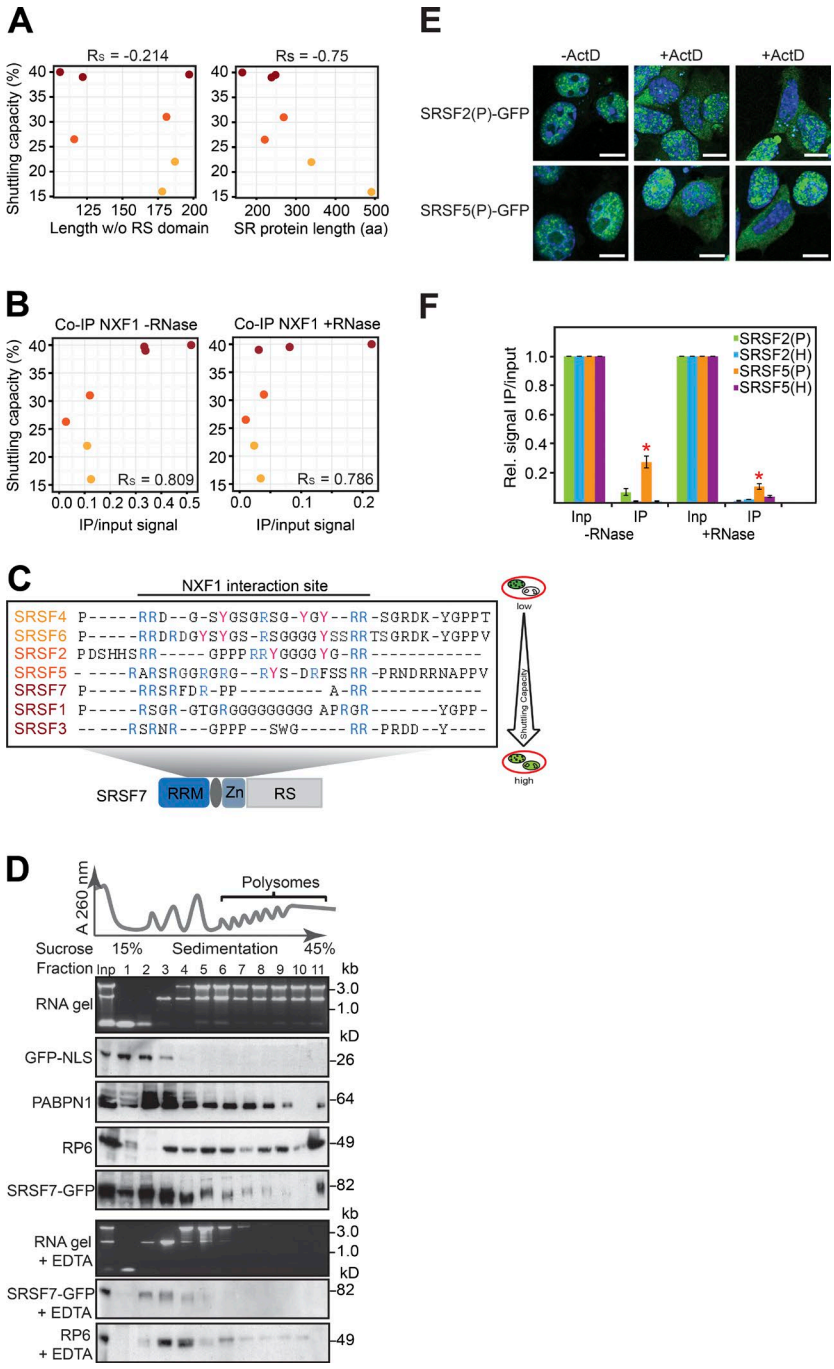

Figure S2. **Shuttling correlations and controls (related to Figs. 2 and 3).** (A) Shuttling capacities of SR proteins are inversely correlated with the lengths of the protein, including the RS domain. Median shuttling capacities quantified from 25 heterokaryons in Fig. 1 D were plotted against the length of each protein with (right) or without (left) the RS domain. Colors indicate shuttling groups of low (SRSF4 and SRSF6; light orange), medium (SRSF2 and SRSF5; dark orange), and high shuttlers (SRSF1, SRSF3, and SRSF7; red; Table S1). Spearman's rank order correlation coefficients are shown above each plot. (B) Shuttling capacities correlate with the extent of NXF1 interaction quantified from semiquantitative reverse coIP experiments ($n = 6$) performed under identical conditions with and without RNase A treatment (Müller-McNicoll et al., 2016). Coloring is as in A. (C) High-shuttling SR proteins lack phosphorylatable tyrosine residues within the NXF1 interaction region. Alignment of putative and verified NXF1 interaction domains from individual SR proteins in the order of shuttling capacities. Coloring of SR proteins is as in A. Arginine residues, potentially important for binding to NXF1, are in bold blue, and tyrosine residues are in pink. (D) Polysome association of SR proteins is independent of the GFP tag. P19 cytoplasmic extracts were fractionated across 15–45% sucrose gradients, and protein distributions were analyzed by Western blotting. RNA gels are shown to confirm the integrity of ribosomes in the fractions. RP6 and PABPN1 serve as controls for a ribosomal protein and an RBP that is associated with polysomes, respectively. RNA gels show that polysomes dissociate after EDTA treatment. SRSF7-GFP and the ribosomal protein RP6 are shifted to lighter fractions. The zinc knuckle containing SRSF7-GFP was reproducibly less abundant after EDTA treatment, most likely because of aggregation or destabilization of the protein in the absence of Zn^{2+} ions, as was reported for other zinc finger proteins (Nyborg and Peersen, 2004). A 260, absorption at 260 nm; Inp, input. (E) P19 cells (P) stably expressing SRSF2-GFP and SRSF5-GFP were treated with 5 µg/ml actinomycin D (ActD), to inhibit transcription by RNA polymerase II, and 20 µg/ml CHX, to block de novo protein synthesis, for 3 h. Cells were fixed and stained with Hoechst before imaging. Merged confocal slices indicate cytoplasmic GFP fluorescence in ActD-treated samples. (F) Quantification of three to eight forward and reverse coIP experiments with SRSF2-GFP and SRSF5-GFP SRSF5 from pluripotent P19 and HeLa (H) cells using FIJI. Values were normalized to baits and inputs. Error bars indicate SEM.

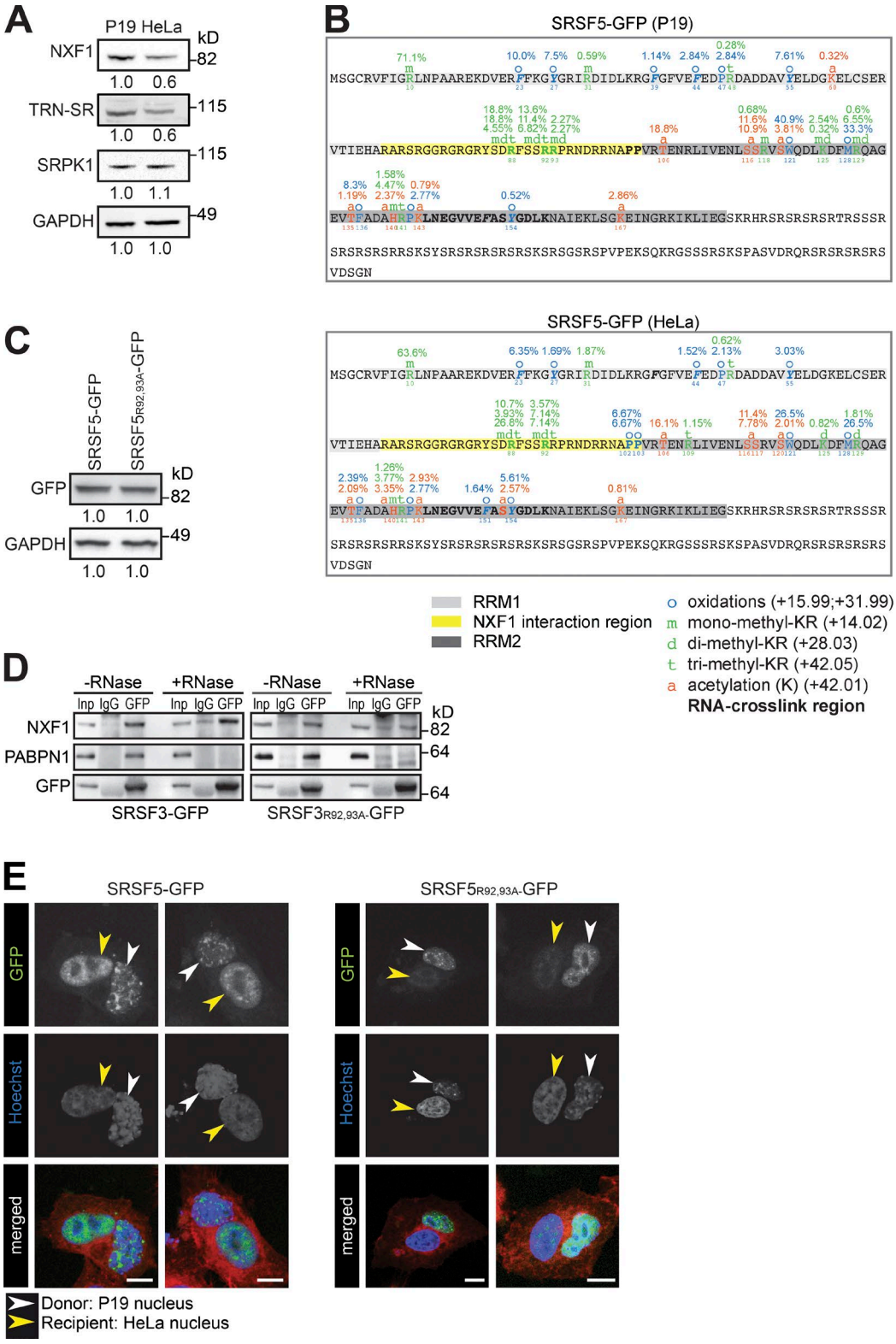

Figure S3. **Methylation of arginine residues within the NXF1 interaction region affects SRSF5 shuttling (related to Fig. 4).** (A) Protein levels of NXF1, TRN-SR, and SRPK1 in pluripotent P19 and HeLa cells were compared by Western blotting and quantified using FIJI. Values were normalized to GAPDH and shown relative to P19 levels. (B) Comparison of PTMs. UV–cross-linked SRSF5-GFP was affinity-purified from P19 and HeLa cells and analyzed by tandem MS to obtain semiquantitative information on the abundance of site-specific PTMs using spectral counting. Summary of eight and six replicates from P19 and HeLa cells, respectively, with the modified amino acids and the percentage of modification compared with all detected peptides indicated above each replicate. RRM1 and RRM2 regions are indicated in gray, and the putative NXF1-interaction region is indicated in yellow. Aromatic residues potentially involved in RNA binding are indicated in italics, and the identified RNA–cross-linked peptide is marked in bold. (C) SRSF5-GFP and SRSF5$_{R92,93A}$-GFP are equally expressed, as estimated by Western blotting using anti-GFP. (D) Representative coIP experiment of SRSF3-GFP and SRSF3$_{R105,106A}$-GFP pulldowns probed for NXF1 interaction. Inp, input. (E) Two representative heterokaryons for SRSF5-GFP and SRSF5$_{R92,92A}$-GFP. Bars, 10 µm.

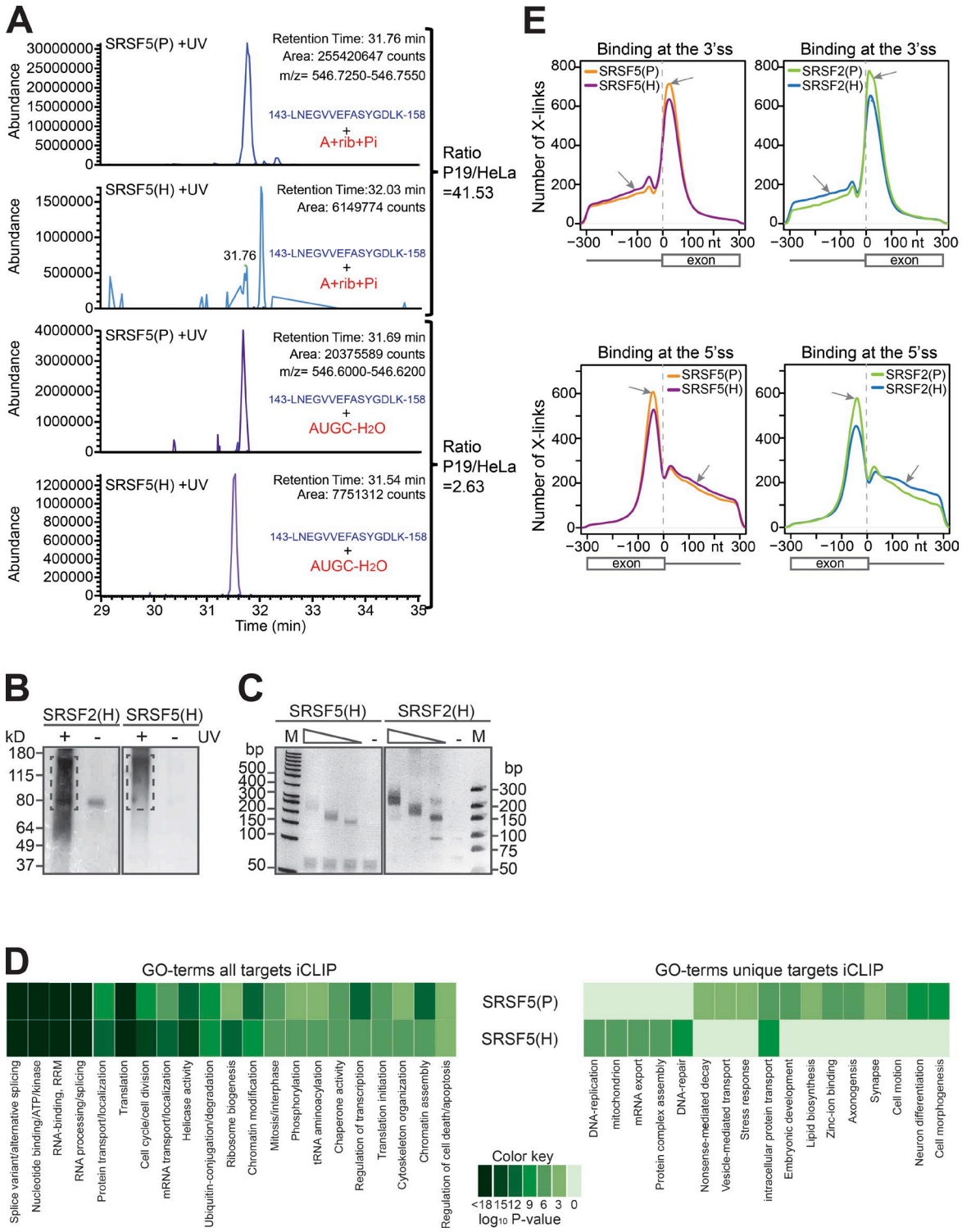

Figure S4. **RNA cross-links and iCLIP to compare RNA binding specificities of SRSF5 in pluripotent P19 and HeLa cells (related to Fig. 5).** (A) Manual screening of nucleic acid cross-link (X-link) spectra from pooled samples (P19 [P], *n* = 7; HeLa [H], *n* = 4) identified one region in RRM2 of SRSF5, 143-LNEGVV EFASYGDLK-158, which is clearly and reproducibly RNA modified in P19 and HeLa cells. Pure peptide peaks are labeled in blue, and RNA-modified fragments and marker ions are in red. The corresponding calculation of the peak area ratios is shown beside the spectra. The top two spectra were extracted from direct injection fractions, and the bottom two spectra with a longer RNA fragment were from the stage-tip fractions. (B) iCLIP of SRSF5- and SRSF2-GFP from HeLa cells. Autoradiogram of radioactively labeled RNA–protein complexes of SRSF2-GFP and SRSF5-GFP after UV cross-linking. UV⁻ samples served as negative controls. Boxed areas indicate cut regions. (C) iCLIP cDNA libraries for GFP-tagged SRSF2 and SRSF5 from HeLa cells. Ramps indicate iCLIP cDNAs corresponding to three different sized ranges of copurified RNA fragments that were cut from B. (D) Gene ontology (GO)-term enrichment analysis for common SRSF5-GFP RNA targets in P19 and HeLa cells (left) and unique SRSF5 RNA targets of P19 and HeLa cells (right) using DAVID ontology cluster analysis (Huang et al., 2009). (E) Shown are cross-links from pooled replicates of SRSF2-GFP and SRSF5-GFP in P19 and HeLa cells that were normalized to similar numbers (see Table S3), mapping to a window of ±300 nt around the 5′ splice site (ss; top) or 3′ splice site (bottom). Arrows point to regions of differential binding in pluripotent P19 and HeLa cells.

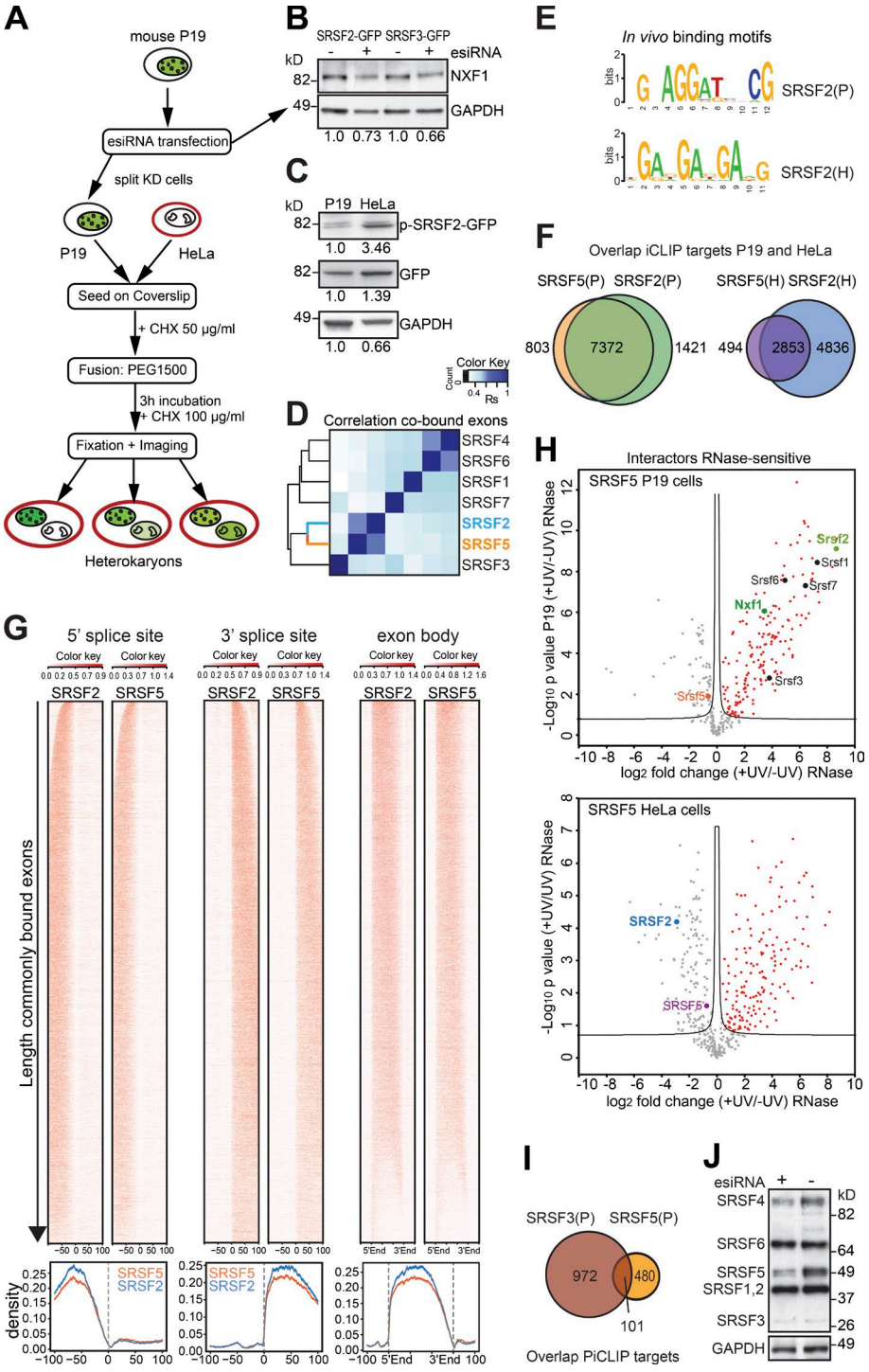

Figure S5. **SRSF2 and SRSF5 bind in close proximity on the same RNA (related to Figs. 6 and 7).** (A) Modified shuttling assay including NXF1 knockdown (KD). Workflow: P19 cells expressing GFP-tagged SRSF2 and SRSF3 proteins were transfected with esiRNAs targeting NXF1 and control esiRNAs. After 24 h, cells were harvested, and one fraction was seeded with CAAX-mCherry HeLa cells on coverslips, fused, fixed, and stained with Hoechst. Two separate experiments have been performed, and 12 heterokaryons each were used for quantification. (B) Western blotting and quantification of NXF1 knockdowns in P19 cells expressing SRSF2-GFP and SRSF3-GFP after 24 h. GAPDH was used as loading control. (C) Representative Western blots and quantifications of SRSF2-GFP phosphorylation level using mAb104. Values were normalized to GAPDH and are shown relative to P19 levels. (D) Hierarchical clustering, using distance correlation and Spearman rank correlation of SR protein cobinding in exons (P19 cells) based on normalized significant iCLIP cross-link events (Müller-McNicoll et al., 2016). (E) In vivo binding motifs (enriched 8-mers) of SRSF2-GFP in P19 (P) and HeLa (H) cells. (F) Overlap of target mRNAs of SRSF2 and SRSF5 in P19 and HeLa cells. (G) Exons shared by SRSF2 and SRSF5 in P19 cells were aligned at their splice sites and ordered by length, and significant cross-link events were visualized in a heat map for a window of 200 nt around 5′ splice sites, 3′ splice sites, or scaled for similar length within the exon body. Summed densities across the heat maps are shown below each one. (H) Interaction between SRSF5 and SRSF2 is RNA independent in HeLa cells. Volcano plot of all proteins detected by tandem MS in RNase T1/A–treated samples with proteins significantly enriched in UV+ samples (red dots; FDR <0.05) for P19 cells ($n = 7$; top) and for HeLa cells ($n = 4$; bottom). SR proteins and NXF1 are indicated. (I) Overlap PiCLIP targets of SRSF3 and SRSF5. (J) Knockdown efficiency of SRSF5 was assessed by Western blotting using mAb104.

Table S1. **Pairwise comparison of shuttling capacities reveal distinct shuttling groups (paired Student's *t* test; related to Fig. 1)**

Protein	PRPF8	SRSF4*	SRSF6*	SRSF2**	SRSF5**	SRSF7***	SRSF1***	SRSF3***	NXF1
PRPF8	1	1.52E-02	3.35E-04	1.34E-05	1.60E-06	4.12E-12	5.40E-14	8.11E-15	1.40E-11
SRSF4*	1.52E-02	1*	1.00E-01*	2.66E-03	1.80E-04	1.47E-08	3.06E-09	2.24E-10	4.43E-10
SRSF6*	3.35E-04	1.00E-01*	1*	3.22E-02	3.11E-03	1.92E-07	4.59E-08	3.67E-09	2.26E-10
SRSF2**	1.34E-05	2.66E-03	3.22E-02	1**	1.89E-01**	1.15E-03	8.09E-04	1.53E-04	2.74E-07
SRSF5**	1.60E-06	1.80E-04	3.11E-03	1.89E-01**	1**	1.99E-02	2.00E-02	5.76E-03	3.36E-06
SRSF7***	4.12E-12	1.47E-08	1.92E-07	1.15E-03	1.99E-02	1***	3.94E-01***	3.57E-01***	5.41E-07
SRSF1***	5.40E-14	3.06E-09	4.59E-08	8.09E-04	2.00E-02	3.94E-01***	1***	2.35E-01***	6.00E-09
SRSF3***	8.11E-15	2.24E-10	3.67E-09	1.53E-04	5.76E-03	3.57E-01***	2.35E-01***	1***	4.69E-08
NXF1	1.40E-11	4.43E-10	2.26E-10	2.74E-07	3.36E-06	5.41E-07	6.00E-09	4.69E-08	1

Colors indicate shuttling groups of low (single asterisk), medium (double asterisk), and high shuttlers (triple asterisk). NXF1 and PRPF8 served as positive and negative controls for nucleocytoplasmic shuttling, respectively.

Table S2. **Replicate correlations iCLIP (counts within binding sites): Spearman's rank order correlation coefficients are shown (related to Fig. 6)**

Protein	Replicate 1	Replicate 2	Replicate 3	Replicate 4
SRSF2(H)	1	0.802625266	0.814868651	
SRSF2(H)	0.802625266	1	0.961800357	
SRSF2(H)	0.814868651	0.961800357	1	
SRSF5(H)	1	0.905146876	0.805427963	0.931898199
SRSF5(H)	0.905146876	1	0.771745966	0.880882852
SRSF5(H)	0.805427963	0.771745966	1	0.788034237
SRSF5(H)	0.931898199	0.880882852	0.788034237	1

H, HeLa cell.

Table S3. **iCLIP mapping statistics (related to Fig. 5)**

	Replicate 1	Replicate 2	Replicate 3	Replicate 4	Combined
SRSF2-GFP(P) iCLIP					
Total reads	30,950,360	17,546,058	27,062,766		75,558,184
Cross-link sites	921,268	92,851	202,860		1,216,979
Binding sites used (FDR <0.05)	101,227	16,038	19,450		136,715
SRSF2-GFP(H) iCLIP					
Total reads	7,282,731	24,813,662	28,204,124		60,300,517
Cross-link sites	43,355	427,538	1,312,151		1,783,089
Binding sites used (FDR <0.05)	5,306	54,993	255,997		316,296
SRSF5-GFP(P) iCLIP					
Total reads	17,792,219	31,709,513	25,605,015		75,106,747
Cross-link sites	258,727	1,414,674	258,983		1,932,384
Binding sites (FDR <0.05)	29,734	289,678	40,306		359,718
SRSF5-GFP(H) iCLIP					
Total reads	17,327,176	7,636,016	27,813,934	19,549,540	72,326,666
Cross-link sites	176,500	43,230	656,520	141,563	1,017,813
Binding sites used (FDR <0.05)	26,450	9,725	67,175	28,103	131,453

Also see the Analysis of iCLIP and RNA-seq data section of Materials and methods. H, HeLa; P, P19.

Table S4 is a separate Excel file showing interactors binding in close proximity to SRSF5-GFP in P19 cells (RNase-sensitive).

Table S5 is a separate Excel file showing interactors binding in close proximity to SRSF5-GFP in P19 cells (partially RNase-resistant).

Table S6 is a separate Excel file showing interactors binding in close proximity to SRSF5-GFP in HeLa cells (RNase-sensitive).

Table S7 is a separate Excel file showing interactors binding in close proximity to SRSF5-GFP in HeLa cells (partially RNase-resistant).

References

Cox, J., and M. Mann. 2008. MaxQuant enables high peptide identification rates, individualized p.p.b.-range mass accuracies and proteome-wide protein quantification. *Nat. Biotechnol.* 26:1367–1372. http://dx.doi.org/10.1038/nbt.1511

Dobin, A., C.A. Davis, F. Schlesinger, J. Drenkow, C. Zaleski, S. Jha, P. Batut, M. Chaisson, and T.R. Gingeras. 2013. STAR: ultrafast universal RNA-seq aligner. *Bioinformatics.* 29:15–21. http://dx.doi.org/10.1093/bioinformatics/bts635

Hargous, Y., G.M. Hautbergue, A.M. Tintaru, L. Skrisovska, A.P. Golovanov, J. Stevenin, L.Y. Lian, S.A. Wilson, and F.H. Allain. 2006. Molecular basis of RNA recognition and TAP binding by the SR proteins SRp20 and 9G8. *EMBO J.* 25:5126–5137. http://dx.doi.org/10.1038/sj.emboj.7601385

Huang, W., B.T. Sherman, and R.A. Lempicki. 2009. Systematic and integrative analysis of large gene lists using DAVID bioinformatics resources. *Nat. Protoc.* 4:44–57. http://dx.doi.org/10.1038/nprot.2008.211

Huppertz, I., J. Attig, A. D'Ambrogio, L.E. Easton, C.R. Sibley, Y. Sugimoto, M. Tajnik, J. König, and J. Ule. 2014. iCLIP: protein-RNA interactions at nucleotide resolution. *Methods.* 65:274–287. http://dx.doi.org/10.1016/j.ymeth.2013.10.011

König, J., K. Zarnack, G. Rot, T. Curk, M. Kayikci, B. Zupan, D.J. Turner, N.M. Luscombe, and J. Ule. 2010. iCLIP reveals the function of hnRNP particles in splicing at individual nucleotide resolution. *Nat. Struct. Mol. Biol.* 17:909–915. http://dx.doi.org/10.1038/nsmb.1838

Larsen, M.R., T.E. Thingholm, O.N. Jensen, P. Roepstorff, and T.J. Jørgensen. 2005. Highly selective enrichment of phosphorylated peptides from peptide mixtures using titanium dioxide microcolumns. *Mol. Cell. Proteomics.* 4:873–886. http://dx.doi.org/10.1074/mcp.T500007-MCP200

Müller-McNicoll, M., V. Botti, A.M. de Jesus Domingues, H. Brandl, O.D. Schwich, M.C. Steiner, T. Curk, I. Poser, K. Zarnack, and K.M. Neugebauer. 2016. SR proteins are NXF1 adaptors that link alternative RNA processing to mRNA export. *Genes Dev.* 30:553–566. http://dx.doi.org/10.1101/gad.276477.115

Nyborg, J.K., and O.B. Peersen. 2004. That zincing feeling: the effects of EDTA on the behaviour of zinc-binding transcriptional regulators. *Biochem. J.* 381:e3–e4. http://dx.doi.org/10.1042/BJ20041096

Rappsilber, J., M. Mann, and Y. Ishihama. 2007. Protocol for micro-purification, enrichment, pre-fractionation and storage of peptides for proteomics using StageTips. *Nat. Protoc.* 2:1896–1906. http://dx.doi.org/10.1038/nprot.2007.261

Richter, F.M., H.H. Hsiao, U. Plessmann, and H. Urlaub. 2009. Enrichment of protein-RNA crosslinks from crude UV-irradiated mixtures for MS analysis by on-line chromatography using titanium dioxide columns. *Biopolymers.* 91:297–309. http://dx.doi.org/10.1002/bip.21139

Surendranath, V., M. Theis, B.H. Habermann, and F. Buchholz. 2013. Designing efficient and specific endoribonuclease-prepared siRNAs. *Methods Mol. Biol.* 942:193–204. http://dx.doi.org/10.1007/978-1-62703-119-6_11

Tintaru, A.M., G.M. Hautbergue, A.M. Hounslow, M.L. Hung, L.Y. Lian, C.J. Craven, and S.A. Wilson. 2007. Structural and functional analysis of RNA and TAP binding to SF2/ASF. *EMBO Rep.* 8:756–762. http://dx.doi.org/10.1038/sj.embor.7401031

Wang, Z., M. Kayikci, M. Briese, K. Zarnack, N.M. Luscombe, G. Rot, B. Zupan, T. Curk, and J. Ule. 2010. iCLIP predicts the dual splicing effects of TIA-RNA interactions. *PLoS Biol.* 8:e1000530. http://dx.doi.org/10.1371/journal.pbio.1000530

Yeo, G.W., N.G. Coufal, T.Y. Liang, G.E. Peng, X.D. Fu, and F.H. Gage. 2009. An RNA code for the FOX2 splicing regulator revealed by mapping RNA-protein interactions in stem cells. *Nat. Struct. Mol. Biol.* 16:130–137. http://dx.doi.org/10.1038/nsmb.1545